Environmental Science Nano

Accepted Manuscript

ROYAL SOCIETY OF CHEMISTRY

rsc.li/es-nano

Nano Impact Statement

Transformations of functional molecular coatings or coronas adsorbed to nanoparticle surfaces will impact the capacity to accurately predict nanoparticle fate and toxicity in natural systems, yet these transformations remain largely unexplored. We investigate the photodegradation of thiolated polyethylene glycol on gold nanoparticles in aqueous media using complementary physicochemical characterization methods. UV irradiation induced rapid coating degradation that significantly decreases colloidal stability, while persistence of residual transformation products result in an altered surface chemistry. The observed phototransformations differ from those for dissolved polymer and prior observations for thiolated self-assembled monolayers irradiated on dried gold substrates in air. Hence, direct *in situ* analysis of the nano-conjugate is necessary to correctly elucidate mechanisms of transformation and to predict their effects on nanoparticle attachment behavior.

Photochemical transformations of thiolated polyethylene glycol coatings on gold nanoparticles

Stacey M. Louie,[1] Justin M. Gorham,[1] Eric A. McGivney,[2,3] Jingyu Liu,[1] Kelvin B. Gregory,[2,3] Vincent A. Hackley[1*]

[1]Materials Measurement Science Division, National Institute of Standards and Technology (NIST), Gaithersburg, MD, 20899

[2]Center for the Environmental Implications of NanoTechnology (CEINT), Carnegie Mellon University, Pittsburgh, PA, 15213

[3]Department of Civil and Environmental Engineering, Carnegie Mellon University, Pittsburgh, PA, 15213

[*]Corresponding author

Phone: 301-975-5790

Email: vince.hackley@nist.gov

Address: 100 Bureau Dr., MS 8520, Gaithersburg, MD, 20899

Abstract

Photochemical reactions can cause significant transformations of manufactured nanomaterials in sunlit environments. While transformations of inorganic nanoparticles (NPs) have been investigated extensively, less attention has been focused on the direct impact of aqueous photochemical reactions on adsorbed organic macromolecules that form the NP corona and strongly influence the surface interactions and reactivity that affect NP transport, fate, and toxicity. Here, we assess the transformations of methoxy polyethylene glycol thiol (mPEGSH) coatings on gold NPs (AuNPs) under controlled UV irradiation. A decrease in the adsorbed layer thickness of polymer was observed within 24 h of UV irradiation, resulting in increased susceptibility of the transformed NPs to aggregation. Surface chemistry analyses, including X-ray photoelectron spectroscopy (XPS), showed loss of the ether groups but persistence of reduced S on the AuNP surface, indicative of a chain scission mechanism yielding different NP surface properties from that of either the initial PEGylated AuNP or the citrate-stabilized AuNP prior to coating with mPEGSH. The transformation of the chemisorbed polymer was compared to that of dissolved mPEGSH in the presence and absence of the Au NPs, as evaluated by liquid chromatography – mass spectrometry (LC-MS). In contrast to the NP-adsorbed coating, the primary observed transformation of the dissolved mPEGSH was thiol oxidation to disulfides without extensive chain scission. This study demonstrates that transformations of adsorbed macromolecular coatings must be considered to accurately predict NP attachment behavior, and hence transport, in environmental systems. Because the corona transformation was not predictable from that of the dissolved polymer, direct NP surface characterization is required to discern the fundamental reactions involved in the photochemical transformation of coatings after sorption to the NP surface.

Introduction

Adsorbed macromolecular coatings or coronas, including synthetic polymers and naturally occurring macromolecules, are ubiquitous on engineered nanoparticle (NP) surfaces. Knowledge of the coating properties, including adsorbed mass, chemistry, and conformation, is required to accurately predict the attachment (e.g., aggregation and deposition), dissolution, reactivity, and biouptake behavior of an engineered NP and ultimately its environmental transport, fate, and toxicity.[1, 2] Beyond characterization of the initial or "pristine" material, physicochemical transformations of the NP and its surface coating must also be assessed to account for changes in surface properties during product use or after NP release into the environment. Previous studies have investigated the desorption of coatings upon long-term storage in aqueous media,[3-6] interactions with proteins or natural organic matter (e.g., displacement or co-adsorption of coatings),[7-9] and biologically mediated degradation of polymeric coatings on NPs.[10, 11]

In this study, we focus on photo-induced transformations that can occur in sunlit surface waters or soils or other light-exposed environments, including wastewater treatment systems utilizing ultraviolet (UV) irradiation. To date, environmental photochemistry studies for engineered nanomaterials have typically focused on transformations of the nanomaterial itself, particularly for silver NPs[12-17] or carbon nanomaterials.[18-20] Photo-transformations of the corona are likely to occur as well. For example, the rate of silver NP aggregation under UV light varies with the type of stabilizer used, which was postulated to result from differences in desorption or degradation of the polymers[17] or the influence of the coating on the generation of reactive O species (ROS);[15] however, thorough characterization of the surface coating transformations was not performed in these studies. Further investigation is needed to identify changes in the

adsorbed coating properties, evaluate the effect of the coating transformations on the NP behavior (e.g., aggregation, as assessed here), and determine the mechanisms involved in coating transformation.

Here, we assess the transformations of a chemisorbed polymer, methoxy PEG thiol (mPEGSH), on aqueous suspensions of gold NPs (AuNPs) under UV irradiation. These PEG-coated NPs (Au-mPEGSH NPs) are of interest for medical applications, where the PEG coating minimizes protein adsorption and increases residence time in the circulatory system.[21, 22] Presently, the AuNP core also serves as a relatively stable model system to probe changes in the corona, because minimal transformation of the AuNP core itself is expected (compared with oxidatively unstable metals like Ag), thus simplifying the analysis of the polymeric coating. Possible coating transformations include complete desorption or oxidation of the thiolated PEG from the NP surface, detachment of polymer fragments by degradation or scission, and chemical transformations (e.g., oxidation) of the polymer without detachment. It is important to distinguish the mechanism of transformation, as it will determine the resulting NP surface properties.

The photochemical transformations of Au-mPEGSH NPs in aqueous suspension have not been reported to our knowledge, but previous studies on related systems suggest that any of the aforementioned mechanisms of coating transformation can occur. UV degradation studies on aqueous solutions of non-thiolated PEG (without NPs) have shown oxidation of the ethers to esters and carboxylic acids, resulting in polymer scission and a decrease in chain length and solution viscosity.[23-25] Photo-oxidation studies have also been performed on thiolated coatings on Au, but these studies typically assessed self-assembled monolayers (SAMs) of low molar mass species (e.g., alkanethiols) on bulk Au substrates that are dried and irradiated in air with

high intensity UV light (e.g., (160 or 3000) mW cm^{-2}.)[26-28] Under these conditions, rapid photo-oxidation to alkanesulfonates or disulfides was observed within minutes to hours.[26-29] On the other hand, the photoreactions of dried alkanethiolate SAMs on Ag substrates under lower intensity irradiation (3 mW cm^{-2}) proceeded by a two-step process of C-S bond scission followed by oxidation of the S to sulfites and sulfates, as determined by Raman spectroscopy.[30] Montague et al. investigated coatings similar to those in the present study, in which oligo(ethylene glycol) (OEG)-terminated SAMs on a flat Au substrate (Au-$S(CH_2)_{11}(OCH_2CH_2)_3OH$) were exposed in air to low intensity UV irradiation (0.3 mW cm^{-2} to 1.25 mW cm^{-2}) centered at 254 nm.[31] Static secondary ion mass spectrometry (SIMS) and X-ray photoelectron spectroscopy (XPS) analyses indicated that the SAM transformation proceeded by rapid oxidation and loss of the OEG end-groups along with slower oxidation of the S to sulfonates within 1 h.

Relative to these previous SAM studies, we provide assessment of thiolated coating degradation in a system more relevant to the environmental nanotechnology community and include several novel aspects. First, the materials and systems used differ from those in previous studies with emphasis on materials of greater concern for environmental implications of nanomaterials: (1) suspended Au NPs were assessed instead of flat Au surfaces; (2) a hydrophilic and hydrated polymeric coating (mPEGSH) commonly used for suspended AuNP formulations was assessed instead of a short-chain alkanethiolate layer; and (3) aqueous conditions were the focus of this study in the UV exposure experiments as well as in the selection of many of the characterization methods used to assess the coating transformation. Furthermore, we provide a more holistic picture of the overall properties of the transformed NPs (e.g., size, presence of residual coating) and explicitly demonstrate the effects of the coating transformation on NP aggregation behavior.

The first objective of this study is to characterize the physicochemical transformations of the mPEGSH coatings on AuNPs in aqueous suspension under UV irradiation (300 nm to 400 nm) comparable to natural sunlight intensities. Complementary methods, including batch dynamic light scattering (DLS), asymmetric flow field flow fractionation with online DLS (A4F-DLS), single particle inductively coupled plasma mass spectrometry (spICP-MS), UV-vis spectroscopy, fluorophore tagging, attenuated total reflectance Fourier transform infrared spectroscopy (ATR-FTIR), and XPS, are applied to evaluate detachment of the adsorbed coating and changes in the surface chemistry of the Au-mPEGSH NPs. The application of this suite of methods, along with thorough comparison against dark controls and UV-exposed cit-AuNP controls, enables discernment of the UV-induced coating transformations from any AuNP core transformations and inference of the transformation mechanism. We then assess the effects of the observed coating loss on the rate of homoaggregation of the AuNPs in environmental test media. The second objective is to compare the UV transformation products of the adsorbed coating and dissolved polymer, the latter of which is assessed for polymer solutions in the presence and absence of the Au-mPEGSH NPs. Chemical assays and liquid chromatography MS (LC-MS) are applied to evaluate changes in the thiol concentration and molar mass distribution. The effects of variability in the oxidation state and purity of the as-received mPEGSH and the presence of inorganic solutes are also briefly explored. Finally, we discuss implications for the environmental fate and transport of polymer-coated NPs.

Experimental section

Materials

Citrate-stabilized AuNPs (cit-AuNPs, nominal 60 nm diameter, BBI Solutions, Cardiff, UK),[¶] were used as the NP core. Stock solutions of mPEGSH of two molar masses, 1 kDa ($mPEGSH_{1000}$) and 5 kDa ($mPEGSH_{5000}$) were prepared at 1 g L^{-1} in deionized (DI) water (Aqua Solutions Type I biological grade water purification system, Jasper, GA). Two sources of the mPEGSH were assessed (Laysan Bio, Arab, AL; Nanocs Inc., Boston, MA): the thiol from one manufacturer was partly oxidized as-received (as determined by Ellman's assay), whereas the highly reduced mPEGSH stock contained a dithiothreitol (DTT) impurity, as discussed below. Additional reagents used in this study are listed in the Supporting Information (SI). Glassware and quartz vials were washed by soaking in a 2 % to 5 % solution of Contrad 70 (Decon Labs, King of Prussia, PA) followed by rinsing with DI water.

Preparation of Au-mPEGSH NPs and cit-AuNP controls

A schematic outlining the AuNP samples and characterization methods used in the present investigation is depicted in Figure 1. Au-mPEGSH NPs were prepared from the cit-AuNPs before each experiment and used within two days of preparation. Adsorption of the coating was performed by adding aliquots of mPEGSH solution (1 g L^{-1}) to the stock cit-AuNP suspension (56 mg L^{-1} as calculated from the size and number concentration reported by the manufacturer) to obtain a final concentration of 28 mg L^{-1} of cit-AuNPs and 200 mg L^{-1} of mPEGSH. The mixture was stirred for (3 to 4) h at room temperature. Amicon ultrafiltration units with a regenerated cellulose membrane (100 kDa molar mass cut-off) (EMD Millipore, Billerica, MA) were used for sample purification and were pre-rinsed three times by centrifuging with DI water at 3000 rpm (≈ 1160 *g*) at 20 °C for 5 min. The Au-mPEGSH NPs were purified

[¶] The identification of any commercial product or trade name does not imply endorsement or recommendation by the National Institute of Standards and Technology.

of excess dissolved polymer and impurities by four cycles of centrifugation (at the same conditions) and resuspension in DI water. The pH was not adjusted or buffered to minimize the addition of potentially photoreactive ions. The measured pH was 7.7 ± 0.2 (n = 7 independently prepared samples) during polymer adsorption and 7.2 ± 0.3 (n = 6) for the Au-mPEGSH suspensions collected after 24 h in dark conditions.

Cit-AuNP controls (without mPEGSH coating) for UV exposure were prepared by centrifuging the cit-AuNP stock as described above to remove impurities (e.g., dissolved citrate) and resuspending the NPs in DI water to a concentration of 28 mg L^{-1}. Significant aggregation of the cit-AuNPs occurs upon extensive washing, so only one centrifugation step was performed.

UV exposure instrumentation

Aqueous suspensions of the Au-mPEGSH NPs were irradiated in quartz vials in a photochemical reactor (RMR-600, Rayonet, Branford, CT) equipped with eight 4 W fluorescent lamps (RMR-3500A, Rayonet) and a fan to maintain the temperature within ≈ 5 °C of room temperature. The UV spectrum reported by the manufacturer was centered at 350 nm and ranged from 300 nm to 400 nm. Dark controls were simultaneously held in the UV reactor in foil-wrapped vials to attain equivalent temperature and atmospheric conditions to the UV-exposed samples. Vials were arranged symmetrically around a merry-go-round sample holder and continuously rotated. The irradiance was estimated to be ≈ 30 W m^{-2} around the cylindrical surface area of the quartz vials (comparable to the total irradiance from 300 nm to 400 nm at sea level for mid-latitude summer conditions at solar noon)[32] in a ferrioxalate actinometry experiment, following the method by Fischer[33] and described in the SI.

Transformations of Au-mPEGSH NPs in DI water

Physicochemical transformations were assessed for the AuNPs coated with 5 kDa mPEGSH (Au-mPEGSH$_{5000}$) and suspended in DI water (Figure 1). The coated AuNPs were characterized for hydrodynamic size by both batch DLS and A4F-DLS, AuNP core size by spICP-MS, electrophoretic mobility (EM) or apparent zeta-potential (ζ), UV-vis absorbance, and surface chemistry (by ATR-FTIR and XPS). Batch DLS size, EM, and UV-vis absorbance were measured on at least three samples prepared independently, from adsorption of the mPEGSH to the cit-AuNPs to purification and UV exposure.

Batch DLS and EM were measured on NP suspensions diluted 1:10 by volume into 1 mmol L^{-1} aqueous sodium bicarbonate solution (adjusted to pH 8 with 0.1 mol L^{-1} nitric acid) on a Zetasizer Nano ZS instrument (Malvern, Westborough, MA). The z-average hydrodynamic diameter (d_z) and polydispersity index (PdI) were determined from cumulants analysis on DLS measurements taken following NIST-NCL Protocol PCC-1[34] and averaged over five measurements per sample at 23 °C. EM was measured using a palladium dip cell (Malvern) with an applied voltage of 3 V, and the average of three measurements per sample was taken. The apparent ζ was computed from the measured EM using the Smoluchowski equation. Batch UV-vis absorbance spectra were collected on a Lambda 750 spectrometer (Perkin Elmer, Waltham, MA) on the undiluted samples (≈ 28 mg L^{-1} of AuNPs) in a quartz microcuvette. Experiments were also performed using a fluorescent, rhodamine-tagged polymer (RhPEGSH) to assess polymer detachment, as described in the SI.

Single particle ICP-MS measurements were conducted on a Thermo X series II quadrupole ICP-MS (Waltham, MA) equipped with a microflow perfluoroalkoxy concentric nebulizer and a glass impact bead spray chamber cooled to 2 ºC, using samples diluted in DI

water to a mass concentration of 0.03 μg L^{-1}. [197] Au intensity was recorded in time resolved analysis (TRA) mode using a dwell time of 10 ms and acquisition time of 360 s. Samples were run in duplicate and more than 450 particle events were recorded in each measurement. NIST AuNP Reference Material 8013 (nominal 60 nm diameter) diluted in water and NIST Standard Reference Material 3121 (Gold Standard Solution) diluted in an acid solution (constituted of 1.0 % mass fraction HCl, 0.04 % mass fraction HNO_3, and 0.5 % mass fraction thiourea) served as NP and dissolved standards, respectively. Data were processed based on established methods[35, 36] to derive particle size distribution and dissolved fraction.

A4F was performed using a Wyatt Eclipse DualTec system (Wyatt Technology, Santa Barbara, CA), with eluent flow provided by an Agilent 1260 Infinity isocratic pump (Agilent Technologies, Santa Clara, CA) equipped with a degasser (ERC 3415α, Shodex, New York, NY) and injection provided by an Agilent 1260 Infinity autosampler. Online detectors included a multiple wavelength UV-vis absorbance detector (Agilent 1260 Infinity) and DLS (Malvern Zetasizer Nano-ZS) operated in flow-mode. The injection, flow, and detector settings are reported in the SI.

ATR-FTIR samples for *in situ*, hydrated UV exposure were prepared from cit-AuNP films dried onto a diamond ATR crystal, followed by adsorption of mPEGSH from solution, rinsing with DI water, application of a quartz coverslip, and UV irradiation. Spectra were collected to monitor polymer adsorption and loss upon UV exposure. Detailed methods are in the SI.

Samples for XPS analysis were prepared by centrifuging (3 to 4) mL of the cit-Au or Au-mPEGSH NP suspensions at 10000 rpm (6700 *g*) for 10 min at room temperature (Eppendorf MiniSpin, Billerica, MA), removing supernatant containing un-adsorbed polymer, resuspending

the NP pellet in DI water, and washing with three additional centrifugation/resuspension cycles at 5000 rpm (1680 *g*) for (5 to 10) min each. The washed pellet was resuspended with DI water to a volume of (30 to 50) μL. The concentrated suspensions were drop-cast onto highly ordered pyrolytic graphite (HOPG) substrates (Structure Probe, Inc., West Chester, PA) and dried under nitrogen in a glove bag.

XP spectra were collected using an Axis Ultra DLD Imaging X-ray Photoelectron Spectrometer from Kratos Analytical (Chestnut Ridge, NY) equipped with a monochromatic Al Kα X-ray source that was operated at 104 W (8 mA; 13 kV). Emitted photoelectrons were collected along the surface normal using slot/hybrid for the iris/aperture settings and analyzed at pass energy 40 eV using a hemispherical analyzer (160 eV for wide range, low energy resolution scans). Spectra for elemental analysis were acquired with a measurement taken every 0.1 eV over predetermined windows to monitor changes in the O (1s), C (1s), S (2p) and Au (4f) regions. Analysis of the acquired spectra was performed using CasaXPS (Teignmouth, UK), as described in the SI. Elemental percentages reported are the average ± one standard deviation of at least three measurements.

Aggregation in environmental test media

Aggregation was assessed for the UV-irradiated Au-mPEGSH$_{5000}$ NPs and the dark and cit-AuNP controls at 2.8 mg L^{-1} in three salt solutions: moderately hard water (MHW)[37] (pH 7.9); artificial seawater (ASW) (ASTM D 1141 without heavy metals, Ricca Chemical, Arlington, TX) (pH 8.1) at 90 % concentration after addition of AuNPs; and a NaCl solution (100 mmol L^{-1} NaCl with 0.9 mmol L^{-1} $NaHCO_3$, pH 8). The compositions of the MHW and

ASW are provided in the SI. DLS measurements were collected every 60 s for 10 min (Malvern Zetasizer Nano ZS) immediately after addition of the NPs to the salt solutions.

Transformations of dissolved mPEGSH

Additional experiments were performed for solutions of 100 mg L^{-1} of dissolved mPEGSH in the presence or absence of 28 mg L^{-1} of suspended Au-mPEGSH NPs (Figure 1), either UV irradiated or under dark conditions for up to 7 d. In addition to $mPEGSH_{5000}$, $mPEGSH_{1000}$ was used because less convoluted LC-MS spectra are obtained. The transformed polymer was collected in the supernatant after pelleting the NPs by centrifugation and characterized by Ellman's assay to quantify reduced thiol (described in SI).

Qualitative LC-MS analysis of the mPEGSH solutions and free polymer in the supernatant of centrifuged Au-mPEGSH suspensions was performed on an Agilent 1100 Series HPLC stack with an Agilent Eclipse XDB-C18 column and an Agilent 6430 Triple Quad MS operated in "MS2 scan" mode. The concentration of polymer was ≈ 100 mg L^{-1} in all samples. An isocratic 50/50 solvent mixture (mobile phase A/mobile phase B) was used, where mobile phase A consisted of 1 mmol L^{-1} ammonium acetate in water, adjusted to pH 8 with ammonium hydroxide, and mobile phase B was acetonitrile. The sample was ionized by electrospray ionization (ESI) in positive mode. The basic pH and additives were chosen for the eluent because the formation of multiply charged species was found to be reduced in comparison to acidic additives, making analysis of the $mPEGSH_{5000}$ feasible. SI Table S1 shows the LC and MS run parameters. All data were analyzed using Agilent MassHunter Qualitative Analysis software.

Results and discussion

Effects of polymer purity and oxidation state

All experiments were performed for the samples prepared using the more highly reduced mPEGSH stock (> 90% expected thiol content, as quantified by Ellman's assay), which was initially presumed to have higher purity than the partially oxidized stock (30% to 40% expected thiol content). However, XPS analyses of the adsorbed coatings on the washed Au-mPEGSH NPs suggested the presence of dithiol impurities that co-adsorbed to the Au NPs from the highly reduced mPEGSH. Personal communication with the manufacturer confirmed that DTT (estimated concentration of ≈ 1 mol %) was added to minimize oxidation of the mPEGSH. DTT is known to adsorb preferentially to (or displace) mPEGSH on AuNPs,[38, 39] so surface characterization (XPS, ATR-FTIR) was performed for samples prepared using the partially oxidized mPEGSH stock without DTT. It is important to note that the main conclusions of this study regarding the transformations of the adsorbed coating on the Au NPs did not change depending on the initial purity of the mPEGSH stock. For example, DLS size and EM measured for the Au-mPEGSH NPs in DI water (*after* removing dissolved polymer and DTT) under dark and UV exposure conditions were similar within one standard deviation (n = 3) for the two mPEGSH stocks. Differences between the stocks were primarily observed as chemical shifts and S concentration changes in the XP spectra and differences in the rate of Au-mPEGSH NP transformation in the presence of excess mPEGSH, as discussed further hereafter.

Physical transformations of Au-mPEGSH NPs in DI water under UV irradiation

The hydrodynamic size and EM or apparent ζ for the cit-AuNP and washed Au-$mPEGSH_{5000}$ NPs are compared in Figure 2 (0 h UV exposure). The z-average hydrodynamic

diameter (d_z) increased from (59.0 ± 0.8) nm with PdI of 0.142 ± 0.007 (n = 3 samples) for the cit-AuNPs to (71.9 ± 1.0) nm with PdI of 0.113 ± 0.012 (n = 3 samples) for the Au-mPEGSH$_{5000}$ NPs, indicating a hydrodynamic layer thickness of ≈ 6.5 nm for the PEG coating. The EM became less negative after PEGylation, which can be attributed to displacement of negatively-charged citrate or an increase in the hydrodynamic drag attributable to the coating.[40] A dense PEG coating will also shift the electrokinetic shear plane outward, causing a reduction in shear plane potential.

Upon UV exposure in DI water, d_z for the Au-mPEGSH$_{5000}$ NPs decreases significantly over the first 9 h and reaches a similar value to the cit-AuNPs by 24 h (Figure 2a,b), i.e, d_z of (59.4 ± 0.7) nm with PdI of 0.145 ± 0.013 (n = 3 samples). These transformations indicate either detachment of the polymer coating or conformational changes resulting in a thinner layer, as is further discussed in the following sections. The Au-mPEGSH$_{5000}$ NPs also attain similar EM to the cit-AuNPs after 24 h UV exposure, consistent with a shift of the shear plane toward the AuNP surface with the decrease in PEG layer thickness and suggesting the presence of residual citrate. In contrast, the dark control and the UV-exposed cit-AuNP control show no significant change in d_z or EM over 24 h. Therefore, the observed physical transformations can be unambiguously attributed to UV-mediated transformations of the polymer coating rather than spontaneous desorption of the coating or transformations of the AuNP core (e.g., dissolution), as further verified by spICP-MS and described below. Extrapolation of the linear trend in either d_z or EM suggests that the UV-mediated transformation reaches completion in ≈ 15 h under the conditions used in this study.

Measurements of d_z were also performed after fractionation by A4F coupled with UV-vis absorbance and light scattering detection (Figure 2c). A4F-DLS should provide a more accurate

and unbiased value for corona thickness (comparing d_z for the pristine and transformed Au-mPEGSH$_{5000}$ NPs to the cit-AuNPs) than batch DLS, particularly if aggregates are present. If significant changes in aggregation state occurred during processing or irradiation, A4F peak shape and width would be expected to change (e.g., decrease in amplitude, broadening or appearance of a shoulder). Here, the chromatograms show a single peak with minimal tailing by UV-vis detection, as well as good overlap of the DLS count rate peak (not shown) with the UV-vis peak, indicating minimal aggregation in the Au-mPEGSH NP suspensions. The online DLS measurements affirm the trend of decreasing hydrodynamic size with UV exposure duration.

spICP-MS measurements were performed to confirm that possible transformations of the AuNP core had minimal effect on the d_z measurements. The mass-based AuNP core size distribution is similar for the Au-mPEGSH$_{5000}$ NPs after 24 h UV exposure compared with the dark control (Figure 3), where the mean diameters are 55.1 nm and 55.7 nm, respectively (n = 2 measurements). Dissolved Au concentrations in both samples are below the limit of quantification. These results indicate that the AuNP cores are colloidally (with respect to aggregation) and chemically (with respect to dissolution) stable after UV exposure for 24 h, as expected.

Batch UV-vis absorbance spectra were collected on the cit-AuNPs and Au-mPEGSH NPs before and after UV irradiation (SI, Figure S1). The intensity and overall shape of the surface plasmon resonance (SPR) peak showed no significant change after 24 h of UV irradiation, further indicating that minimal loss, aggregation, or dissolution of the AuNP cores occurred. A small red shift ($\Delta \approx 2$ nm) of the SPR peak was observed upon coating the cit-AuNPs with mPEGSH$_{5000}$, consistent with previously reported observations.[41] Upon UV irradiation, the SPR peak of the transformed Au-mPEGSH$_{5000}$ NPs shows a blue shift toward the initial cit-AuNP

SPR peak that is not observed in the dark controls (SI, Figure S1) and which may be attributable to loss of the polymer coating.

Additional experiments were performed using AuNPs coated with a fluorescent, rhodamine-labeled polymer (Au-RhPEGSH), as described in the SI. Briefly, a small but significantly higher quantity of rhodamine was measured in the supernatant of the UV-irradiated Au-RhPEGSH NPs compared to the dark control (after pelleting the NPs by centrifugation), suggesting detachment of rhodamine-containing PEG or PEG fragments under UV light (SI, Figure S2).

Transformation of Au-mPEGSH NP surface chemistry in DI water under UV irradiation

The surface chemistry of the Au-mPEGSH$_{5000}$ NPs was directly assessed by ATR-FTIR spectroscopy and XPS. As discussed above, the partially oxidized mPEGSH$_{5000}$ stock was used to prepare the Au-mPEGSH$_{5000}$ NPs for the surface characterization presented here, with XPS results for the mPEGSH$_{5000}$ with DTT impurity presented in the SI.

ATR-FTIR spectroscopy showed a decrease in the absorbance peaks attributable to the PEG ether groups upon *in situ* UV irradiation of the hydrated, mPEGSH-coated AuNP film on the diamond FTIR substrate (SI Figure S3), suggesting detachment of PEG from the NPs. However, the hypothesized mechanisms for polymer degradation (chain scission versus S oxidation) could not be distinguished because the C-S bonds do not exhibit appreciable IR absorbance. Furthermore, the possibility for detachment or rearrangement of the NPs on the FTIR substrate resulted in uncertainty in the semi-quantitative analysis of the *in situ* FTIR data.

XPS was used to further characterize transformations of the surface (sampling depth ≈ 10 nm) of the washed, pelleted Au-mPEGSH$_{5000}$ NPs in the presence and absence of UV radiation

(Figure 4). The photo-induced surface transformations were monitored by observation of the total S content, or S (2p) region, with respect to the AuNP, or Au (4f) region. For the washed, pelleted, Au-mPEGSH$_{5000}$ NP samples, the S (2p) region was characterized as a peak around (161.9 to 162.2) eV, which was significantly lower than the primary S peak for the mPEGSH$_{5000}$ control at (163.8 to 164.1) eV, regardless of presence or absence of UV exposure (SI Figure S4). Additionally, there was no observable SO_x component on the AuNP surface that was minimally present on the mPEGSH$_{5000}$ control. This suggests the presence of a more reduced S species on the Au surface, presumably as a thiolate species, which is not further transformed by UV exposure.

Figure 4 evaluates the (a) S and (b) O content at the surface relative to the measured Au photoelectron intensity for the Au-mPEGSH$_{5000}$ NP before and after 24 h of UV/dark exposure and their controls. Figure 4a demonstrates that the majority of the S at the AuNP surface derives from the mPEGSH$_{5000}$ and that, regardless of the exposure of the Au-mPEGSH$_{5000}$ NP to 24 h UV irradiation or storage in the dark, the S content did not significantly increase or decrease. This is consistent with the results from the DTT contaminated mPEGSH$_{5000}$ for the first 24 h of exposure, albeit prolonged exposures suggest a loss in S was possible (SI Figure S5).

Figure 4b demonstrates that the O content at the surface significantly increases upon coating of the cit-AuNP with the mPEGSH$_{5000}$, which is consistent with a surface functionalized with a long, straight chain polymer composed of multiple ethoxy (-CH_2-CH_2-O-) monomeric units as opposed to a small molecule like citrate. Upon 24 h of UV exposure, the surface O content decreases back to the initial cit-AuNP levels, as indicated by the O:Au plot. The 24 h dark control confirmed that the phenomenon observed was indeed due to the UV exposure. The evolution of the mPEGSH$_{5000}$ modified AuNP surface due to UV exposure suggests that the PEG

chain is being degraded and removed from the surface while a small residual thiolate component (the active site of the mPEGSH chain) remains bound to the surface. This is consistent with the C (1s) results (see SI Figure S4), which reflect a loss of the PEG associated C due to UV exposure.

Overall, UV irradiation of the Au-mPEGSH NPs induced loss of ether-containing PEG but persistence of a thiolated transformation product on the NP surface, yielding a surface chemistry different from that of either the cit-AuNPs or the initially PEGylated NPs. Likely, scission occurred by oxidation and cleavage at the ether bonds, as observed previously for dried OEG-terminated SAMs on Au (Au-S(CH_2)$_{11}$(OCH_2CH_2)$_3$OH) [31] and UV-irradiated solutions of non-thiolated polyethylene glycol,[23, 25] but direct measurements identifying formation of terminal hydroxyl or carboxyl groups on the transformed PEG thiolate coating would be required to confirm this mechanism. Scission of the C–S bond is another possible mechanism, as previously shown for an alkanethiolate SAM on Ag[30] using Raman spectroscopy, which is sensitive to the C–S bond[42, 43] and will be pursued in future work for the AuNPs evaluated here. Scission of the polymer is consistent with the observed decrease in layer thickness (Figure 2a): the residual thiolate component on the AuNP surface is expected to contribute minimally (< 1 nm) to the NP size, and the degraded PEG fragments are expected to dissolve with minimal physisorption onto the NP, where d_z for AuNPs incubated in 5 kDa mPEGOH (Nanocs) was similar within one standard deviation (n = 2 samples) to that of the cit-AuNPs.

Notably, oxidation or desorption of the S from the Au NPs was not observed within 24 h under the aqueous conditions tested here, in contrast to studies on dried SAMs on Au that were irradiated in air,[26-29] where even the OEG-terminated SAMs showed significant sulfonate formation within 1 h under low irradiances (e.g., 3 W m^{-2}).[31] The slow rate of S oxidation

observed here may be attributable to the low O_2 concentrations in water relative to air, thicker layer of PEG coating in contrast to short-chain thiolated SAMs, or the more stable Au-thiolate bonds formed on nanoscale Au as opposed to bulk Au, as observed in previous studies and attributed to higher thiol adsorption energy at substrate defect sites on nanoscale Au.[44]

Effects of UV-induced transformations on AuNP aggregation behavior

The aggregation behavior of the Au-mPEGSH$_{5000}$ NPs is compared for the 24 h UV exposed samples, dark Au-mPEGSH$_{5000}$ controls, and the cit-AuNPs after addition of the NPs into two environmental test media, MHW and ASW (Figure 5), as well as a NaCl solution (SI Figure S7). In each of the test media, the control (dark) Au-mPEGSH$_{5000}$ NPs show good colloidal stability, whereas those collected after 24 h UV exposure show similar aggregation rates to the cit-AuNPs. These results are consistent with loss of steric stabilization upon detachment of the polymer coating, and they demonstrate that UV-induced coating transformations can significantly change the attachment behavior of the Au-mPEGSH$_{5000}$ NPs.

Transformations of mPEGSH solutions in the presence and absence of Au-mPEGSH NPs

Solutions of 100 mg L^{-1} of mPEGSH were irradiated for up to 7 d in the presence or absence of suspended Au-mPEGSH NPs (Figure 1). In these systems, we initially hypothesized that the excess mPEGSH from solution would continually adsorb and transform at the surface of the AuNP, resulting in the accumulation of degraded corona fragments in solution, as previously proposed in a study assessing CdSe NPs exposed to UV light in solutions of mercaptopropionic acid.[45] However, in this study, the transformation products of the dissolved mPEGSH are not

consistent with those of the adsorbed corona, so the transformations described hereafter likely represent solution-phase rather than adsorbed-phase reactions.

For polymer characterization, we distinguish thiol oxidation from chain scission by assessing the thiol concentration and molar mass distribution of the mPEGSH over 7 d UV exposure in the presence or absence of the Au-mPEGSH NPs. Quantification of the thiol concentration by Ellman's assay demonstrated a significant decrease in thiol concentration in all samples except the dark NP-free controls (Figure 6a). The thiol concentration decreased more rapidly in the presence of the UV-irradiated Au NPs than in any of the control samples. However, the thiol loss after 7 days for the UV-irradiated Au NPs ((13.7 ± 3.5) μmol L^{-1} relative to the dark NP-free control; n = 3 samples) is not significantly greater than the summed thiol losses attributable separately to UV exposure (without Au NPs; figure 6a, empty diamonds) and the presence of the Au NPs (dark; figure 6a, dark squares) (summed loss of (9.6 ± 2.4) μmol L^{-1}, n = 3 samples). Hence, a synergistic effect of UV irradiation and Au NPs together, e.g., via photocatalytic production of ROS by the Au NPs could not be definitively established.

LC-MS was used for qualitative assessment of transformed species in the dissolved mPEGSH samples. Samples for LC-MS were reacted with Ellman's reagent, 5,5'-dithiobis-(2-nitrobenzoic acid) (DTNB), immediately after collection to stabilize thiols in the mPEGSH as a mixed disulfide (mPEGS-TNB). The chromatograms show two peaks in the total ion count (Figure 6b), and the eluting species were characterized by MS (Figure 7). The molar mass was estimated by multiplying the mass-to-charge (m/z) by the charge state, which was determined by comparing the spacing between peaks in the m/z distributions (where each peak represents an oligomer of PEG) with the mass of the PEG monomer (44 Da). The first eluting peak corresponded to the TNB-tagged mPEGSH ($m \approx 5$ kDa), and the second peak corresponded to

disulfides formed between two mPEGSH molecules ($m \approx 10$ kDa). The highest contribution of the disulfides was observed after 7 d UV irradiation in the presence of the Au-mPEGSH NPs, consistent with the results of Ellman's assay suggesting thiol oxidation. No chain scission products could be positively identified, and the m/z distribution for the main peaks in the mass spectrum did not shift to lower values upon UV irradiation compared to the stock mPEGSH solution (SI Figure S8).

Additional analyses were performed to further probe for transformation products of the dissolved mPEGSH. More highly oxidized S species (SO_x) were observed by XPS for $mPEGSH_{5000}$, but results were highly variable on an experiment-by-experiment basis, presumably because of sample preparation issues (e.g., O_2 exposure during drying and sample transfer). Experiments were also performed using $mPEGSH_{1000}$ because it exhibits less convoluted mass spectra with primarily singly- and doubly-charged ions: while the UV-irradiated AuNPs had a less significant effect on the rate of thiol loss for $mPEGSH_{1000}$ than for $mPEGSH_{5000}$ (SI Figure S10), LC-MS again showed the presence of disulfides and no evidence of significant chain scission for $mPEGSH_{1000}$ (SI Figure S11). Finally, total organic C analysis (described in the SI) confirmed no significant loss of C (e.g., by volatilization) that would preclude observation of chain scission products.

Comparison of transformations of the adsorbed and dissolved polymer

The transformations observed for the dissolved mPEGSH were not consistent with those observed for the adsorbed corona on the Au-mPEGSH NPs: the XPS results for the adsorbed corona suggest that polymer loss from the AuNPs results from scission of the polymer (not S oxidation), whereas the most significant transformation observed by LC-MS for the dissolved

mPEGSH was thiol oxidation rather than chain scission. We propose three possible explanations for why corona degradation products were not observed in the polymer solutions in the presence of Au-mPEGSH NPs. First, the concentration of polymer in the adsorbed corona (≈ 0.2 mg L^{-1}, as estimated from the reported saturation adsorbed mass for 60 nm Au NPs coated with 5 kDa mPEGSH)[7] is low relative to the dissolved polymer concentration (100 mg L^{-1}). Second, minimal exchange of adsorbed and dissolved mPEGSH may have occurred: DLS measurements suggest that residual transformed coating on the Au-mPEGSH surface can block adsorption of dissolved polymer that occurs on cit-AuNPs (SI Figure S12a). Third, the free thiols in the mPEGSH solution, which can scavenge ROS, likely react preferentially to the ether groups to reduce the rate of chain scission and corona degradation, as suggested by differences in the rate of change in d_z for the Au-mPEGSH NPs in DI water (Figure 2a) and solutions of partially oxidized or highly reduced mPEGSH (SI Figure S12). Additional experiments with isotopically- or fluorescently-labeled polymers would be useful to directly assess corona loss and exchange of polymer for the Au-mPEGSH NPs in dissolved polymer solutions.

Effect of indirect photochemistry in natural environments

To further understand the photoreactivity of the Au-mPEGSH NPs, the effect of nitrate (NO_3^-) and hydrogen peroxide (H_2O_2) was also tested (SI Figure S13) to investigate the possible role of indirect photoreactions (i.e., reaction of the Au-mPEGSH with ROS produced by external photosensitizers) that can occur in the natural environment. H_2O_2 significantly accelerated degradation of the coating under UV light, but the estimated rate of hydroxyl radical ($HO^{\bullet}$) production from H_2O_2 used here was higher than expected to be relevant for natural environments. On the other hand, the rate of coating loss decreased in the presence of $NaHCO_3$

(1 mmol L^{-1}), which may be indicative of ROS scavenging by HCO_3^-.[32] The ability of natural organic matter (NOM) to absorb UV irradiation or scavenge or produce ROS should also be considered but will require more thorough experimentation and characterization because of the heterogeneity and supramolecular or macromolecular properties of the NOM. Overall, we expect that UV-induced corona degradation in natural waters will primarily be driven by direct photoreactions of the Au-mPEGSH NPs but may be slower than measured in DI water here.

Conclusions and implications

This research demonstrates that polymeric coatings on NPs can undergo significant photo-induced transformations that must be considered to accurately predict NP fate and transport in sunlit environments. More specifically:

- Significant degradation of thiolated methyl-PEG coating on AuNPs occurs under UV irradiation, resulting in higher susceptibility to aggregation in moderate and high ionic strength media. Laboratory experiments performed using only the "pristine" mPEGSH-coated AuNPs may then overestimate the colloidal stability and mobility of these NPs in sunlit environments.
- Thiolated corona fragments remained on the AuNP surface after the UV-induced transformation, resulting in a surface coating different from that of either the native citrate capped AuNPs or the thiol-PEGylated AuNPs. The effects of the modified NP surface chemistry on the environmental and biological interactions of the NP surface (e.g., biouptake, toxicity, and adsorption of natural organic matter or biomacromolecules) should be further investigated.

- The adsorbed corona appears to undergo different transformations than the dissolved mPEGSH, which showed primarily thiol oxidation rather than PEG scission. Therefore, assessment of dissolved polymer transformations is not a suitable or sufficient approach to identify the corona transformations in this system.

This study is the first, to our knowledge, to thoroughly evaluate the phototransformations of thiol-PEG coatings on AuNPs in aqueous suspension. Importantly, the slow oxidation of S over 24 h to 7 d of UV exposure (and hence significance of the partially-degraded coating state) would not have been straightforward to predict from previous photodegradation studies assessing dried alkanethiolate[26-29] or OEG-terminated[31] SAMs on bulk Au substrates, which showed rapid photo-oxidation of the S to sulfonates or sulfates within 1 h, even at low irradiance levels.[31] This oxidation would result in more complete desorption of the thiolated PEG and restoration of a clean Au NP surface, which was not observed here. Additional study is needed for the Au-mPEGSH NPs as has previously been performed for SAMs on Au as reviewed by Vericat et al.[44] to assess the roles of bulk versus NP reactivity, O_2 levels, hydration, coating layer thickness, and UV wavelength and irradiance, and the relative importance of these parameters.

These results highlight the need for the application or development of sensitive methods to characterize the NP surface and the low concentrations of degradation products released directly from the surface coating. Both experimental and theoretical (e.g., density functional theory modeling) investigation of the transformations of a range of NP types and polymers with different chemistries and binding mechanisms is needed to more broadly predict photochemical transformations of adsorbed coatings on NPs. Future studies will provide a more thorough testing and modeling of the effects of environmental parameters, such as water chemistry,

dissolved oxygen concentration (where oxidative degradation is expected to be hindered in deaerated or reducing environments), and NOM composition (considering both the interactions of NOM with light and its ability to sorb to the transformed NP surface). Finally, comparison of the rates and products of UV-induced transformations with other chemical, thermal, or biologically-mediated degradation processes (e.g., oxidation by ROS produced biologically[46] or in the pore water of subsurface sediments exposed to fluctuating redox conditions[47]) is also needed to achieve a holistic assessment of corona transformations in the natural environment.

Acknowledgments

We acknowledge and thank Brian Sim for performing the photosensitizer experiments with funding support through the NIST summer undergraduate research fellowship (SURF) program. We also thank Richard Gates for use of the ATR-FTIR instrument, Mike Winchester for use of the ICP-MS instrument, Stephanie Watson for providing the TOC instrument, and John Pettibone, Yamil Simon, Jeff Clogston, and Hind El Hadri for helpful advice. We acknowledge the National Research Council for a postdoctoral fellowship to SML. For EAM, we acknowledge the National Science Foundation (NSF) Integrative Graduate Education and Research Traineeship in Nanotechnology Environmental Effects and Policy fellowship program (DGE0966227) and the NSF and EPA funding under NSF Cooperative Agreement EF-1266252, Center for the Environmental Implications of NanoTechnology (CEINT). Finally, we acknowledge the nanoEHS initiative program at NIST, coordinated by Debra Kaiser, for providing long term funding support that in part enabled this study.

References

1. S. M. Louie, R. D. Tilton and G. V. Lowry, *Environ. Sci. Nano*, 2016.
2. A. E. Nel, L. Madler, D. Velegol, T. Xia, E. M. V. Hoek, P. Somasundaran, F. Klaessig, V. Castranova and M. Thompson, *Nat Mater*, 2009, **8**, 543-557.
3. H. J. Kim, T. Phenrat, R. D. Tilton and G. V. Lowry, *Environ. Sci. Technol.*, 2009, **43**, 3824-3830.
4. D.-H. Tsai, Y.-F. Lu, F. DelRio, T. Cho, S. Guha, M. Zachariah, F. Zhang, A. Allen and V. Hackley, *Anal. Bioanal. Chem.*, 2015, 1-12.
5. E. J. Petersen, T. B. Henry, J. Zhao, R. I. MacCuspie, T. L. Kirschling, M. A. Dobrovolskaia, V. Hackley, B. S. Xing and J. C. White, *Environ. Sci. Technol.*, 2014, **48**, 4226-4246.
6. E. J. Petersen, R. A. Pinto, D. J. Mai, P. F. Landrum and W. J. Weber, *Environ. Sci. Technol.*, 2011, **45**, 1133-1138.
7. D. H. Tsai, M. Davila-Morris, F. W. DelRio, S. Guha, M. R. Zachariah and V. A. Hackley, *Langmuir*, 2011, **27**, 9302-9313.
8. B. Pelaz, P. del Pino, P. Maffre, R. Hartmann, M. Gallego, S. Rivera-Fernandez, J. M. de la Fuente, G. U. Nienhaus and W. J. Parak, *ACS Nano*, 2015, **9**, 6996-7008.
9. B. L. T. Lau, W. C. Hockaday, K. Ikuma, O. Furman and A. W. Decho, *Colloids Surf., A*, 2013, **435**, 22-27.
10. W. G. Kreyling, A. M. Abdelmonem, Z. Ali, F. Alves, M. Geiser, N. Haberl, R. Hartmann, S. Hirn, D. J. de Aberasturi, K. Kantner, G. Khadem-Saba, J. M. Montenegro, J. Rejman, T. Rojo, I. R. de Larramendi, R. Ufartes, A. Wenk and W. J. Parak, *Nat. Nanotechnol.*, 2015, **10**, 619-623.
11. T. L. Kirschling, P. L. Golas, J. M. Unrine, K. Matyjaszewski, K. B. Gregory, G. V. Lowry and R. D. Tilton, *Environ. Sci. Technol.*, 2011, **45**, 5253-5259.
12. S. J. Yu, Y. G. Yin, J. B. Chao, M. H. Shen and J. F. Liu, *Environ. Sci. Technol.*, 2014, **48**, 403-411.
13. A. R. Poda, A. J. Kennedy, M. F. Cuddy and A. J. Bednar, *J. Nanopart. Res.*, 2013, **15**.
14. J. Y. Liu, Z. Y. Wang, F. D. Liu, A. B. Kane and R. H. Hurt, *ACS Nano*, 2012, **6**, 9887-9899.
15. Y. Li, W. Zhang, J. F. Niu and Y. S. Chen, *Environ. Sci. Technol.*, 2013, **47**, 10293-10301.
16. J. M. Gorham, R. I. MacCuspie, K. L. Klein, D. H. Fairbrother and R. D. Holbrook, *J. Nanopart. Res.*, 2012, **14**.
17. Y. W. Cheng, L. Y. Yin, S. H. Lin, M. Wiesner, E. Bernhardt and J. Liu, *J. Phys. Chem. C*, 2011, **115**, 4425-4432.
18. W. C. Hou, L. J. Kong, K. A. Wepasnick, R. G. Zepp, D. H. Fairbrother and C. T. Jafvert, *Environ. Sci. Technol.*, 2010, **44**, 8121-8127.
19. X. L. Qu, P. J. J. Alvarez and Q. L. Li, *Environ. Sci. Technol.*, 2013, **47**, 14080-14088.
20. J. L. Bitter, J. Yang, S. B. Milani, C. T. Jafvert and D. H. Fairbrother, *Environ-Sci Nano*, 2014, **1**, 324-337.
21. J. V. Jokerst, T. Lobovkina, R. N. Zare and S. S. Gambhir, *Nanomedicine-Uk*, 2011, **6**, 715-728.
22. K. Knop, R. Hoogenboom, D. Fischer and U. S. Schubert, *Angew Chem Int Edit*, 2010, **49**, 6288-6308.
23. F. Hassouna, S. Morlat-Therias, G. Mailhot and J. L. Gardette, *Polym. Degrad. Stabil.*, 2007, **92**, 2042-2050.
24. C. W. Mcgary, *J. Polym. Sci.*, 1960, **46**, 51-57.
25. S. Morlat and J. L. Gardette, *Polymer*, 2003, **44**, 7891-7897.
26. J. Y. Huang and J. C. Hemminger, *J. Am. Chem. Soc.*, 1993, **115**, 3342-3343.
27. G. Gillen, J. Bennett, M. J. Tarlov and F. Burgess, *Anal. Chem.*, 1994, **66**, 2170-2174.
28. M. J. Tarlov, D. R. F. Burgess and G. Gillen, *J. Am. Chem. Soc.*, 1993, **115**, 5305-5306.
29. E. Cooper and G. J. Leggett, *Langmuir*, 1998, **14**, 4795-4801.
30. M. Lewis, M. Tarlov and K. Carron, *J. Am. Chem. Soc.*, 1995, **117**, 9574-9575.

31. M. Montague, R. E. Ducker, K. S. L. Chong, R. J. Manning, F. J. M. Rutten, M. C. Davies and G. J. Leggett, *Langmuir*, 2007, **23**, 7328-7337.
32. D. Vione, M. Minella, V. Maurino and C. Minero, *Chem. Eur. J.*, 2014, **20**, 10590-10606.
33. E. Fischer, *EPA Newsletter*, 1984, **21**, 33-34.
34. V. A. Hackley and J. D. Clogston, *Measuring the size of nanoparticles in aqueous media using batch-mode dynamic light scattering*, Report Special Publication (NIST SP) 1200-6, 2015.
35. J. Y. Liu, K. E. Murphy, R. I. MacCuspie and M. R. Winchester, *Anal. Chem.*, 2014, **86**, 3405-3414.
36. H. E. Pace, N. J. Rogers, C. Jarolimek, V. A. Coleman, C. P. Higgins and J. F. Ranville, *Anal. Chem.*, 2011, **83**, 9361-9369.
37. J. S. Taurozzi, V. A. Hackley and M. R. Wiesner, *Preparation of nanoscale TiO_2 dispersions in an environmental matrix for eco-toxicological assessment*, Report Special Publication (NIST SP) 1200-5, 2012.
38. D. H. Tsai, M. P. Shelton, F. W. DelRio, S. Elzey, S. Guha, M. R. Zachariah and V. A. Hackley, *Anal. Bioanal. Chem.*, 2012, **404**, 3015-3023.
39. M. C. Smith, R. M. Crist, J. D. Clogston and S. E. McNeil, *Anal. Bioanal. Chem.*, 2015, **407**, 3705-3716.
40. T. L. Doane, C. H. Chuang, R. J. Hill and C. Burda, *Acc. Chem. Res.*, 2012, **45**, 317-326.
41. K. Rahme, L. Chen, R. G. Hobbs, M. A. Morris, C. O'Driscoll and J. D. Holmes, *RSC Adv.*, 2013, **3**, 6085-6094.
42. M. A. Bryant and J. E. Pemberton, *J. Am. Chem. Soc.*, 1991, **113**, 8284-8293.
43. M. H. Schoenfisch and J. E. Pemberton, *J. Am. Chem. Soc.*, 1998, **120**, 4502-4513.
44. C. Vericat, M. E. Vela, G. Benitez, P. Carro and R. C. Salvarezza, *Chemical Society Reviews*, **39**, 1805-1834.
45. J. Aldana, Y. A. Wang and X. G. Peng, *J. Am. Chem. Soc.*, 2001, **123**, 8844-8850.
46. T. Zhang, C. M. Hansel, B. M. Voelker and C. H. Lamborg, *Environ. Sci. Technol.*, 2016.
47. M. Tong, S. Yuan, S. Ma, M. Jin, D. Liu, D. Cheng, X. Liu, Y. Gan and Y. Wang, *Environ. Sci. Technol.*

Figures

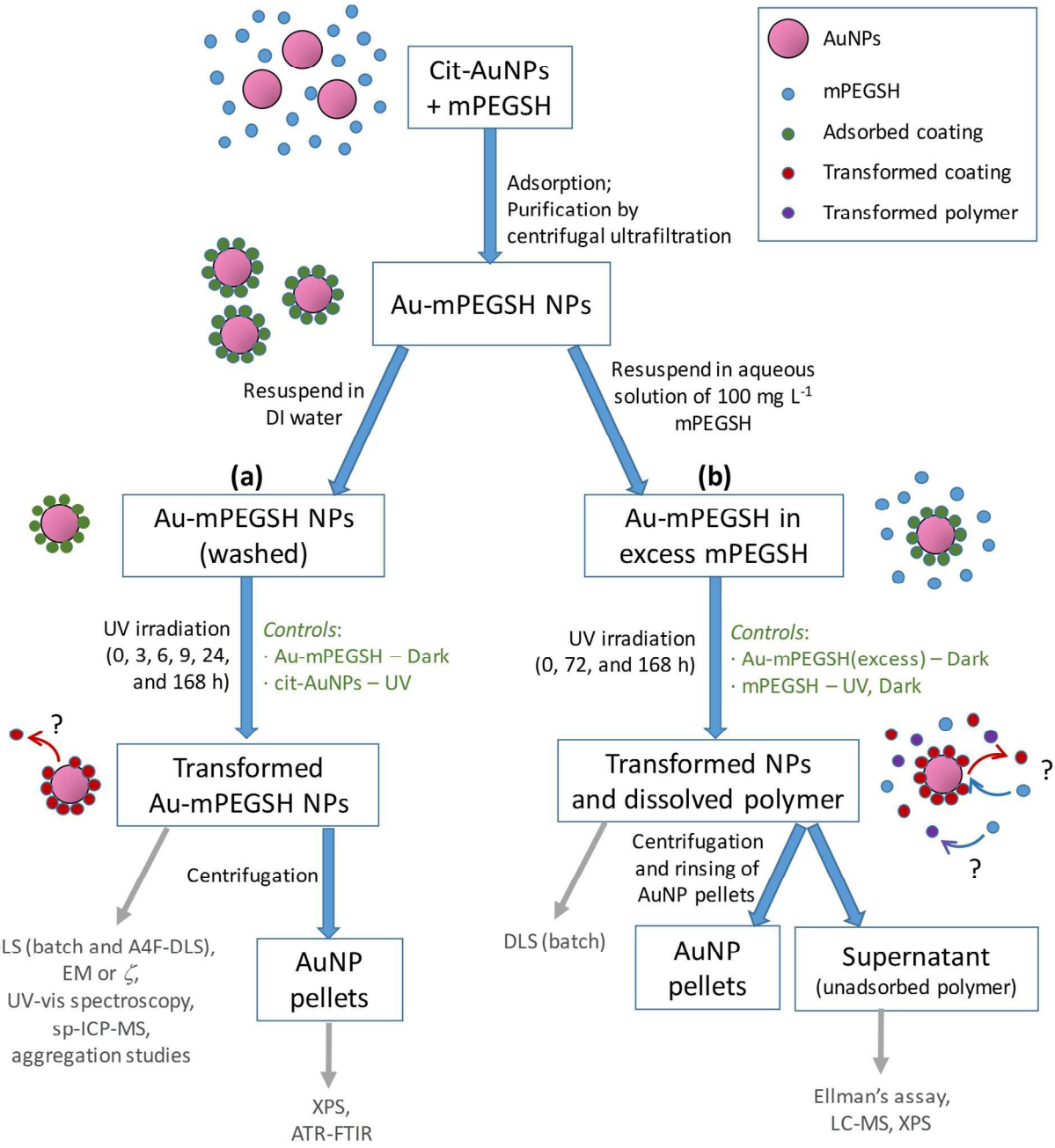

Figure 1. Schematic of the sample preparation, UV exposure experiments, and characterization methods applied. (a) The washed Au-mPEGSH NPs were suspended in DI water to assess transformations of the corona on the AuNP surface after UV exposure. (b) Additional experiments were performed in dissolved polymer solutions, where both the NPs and dissolved polymer in the supernatant were characterized.

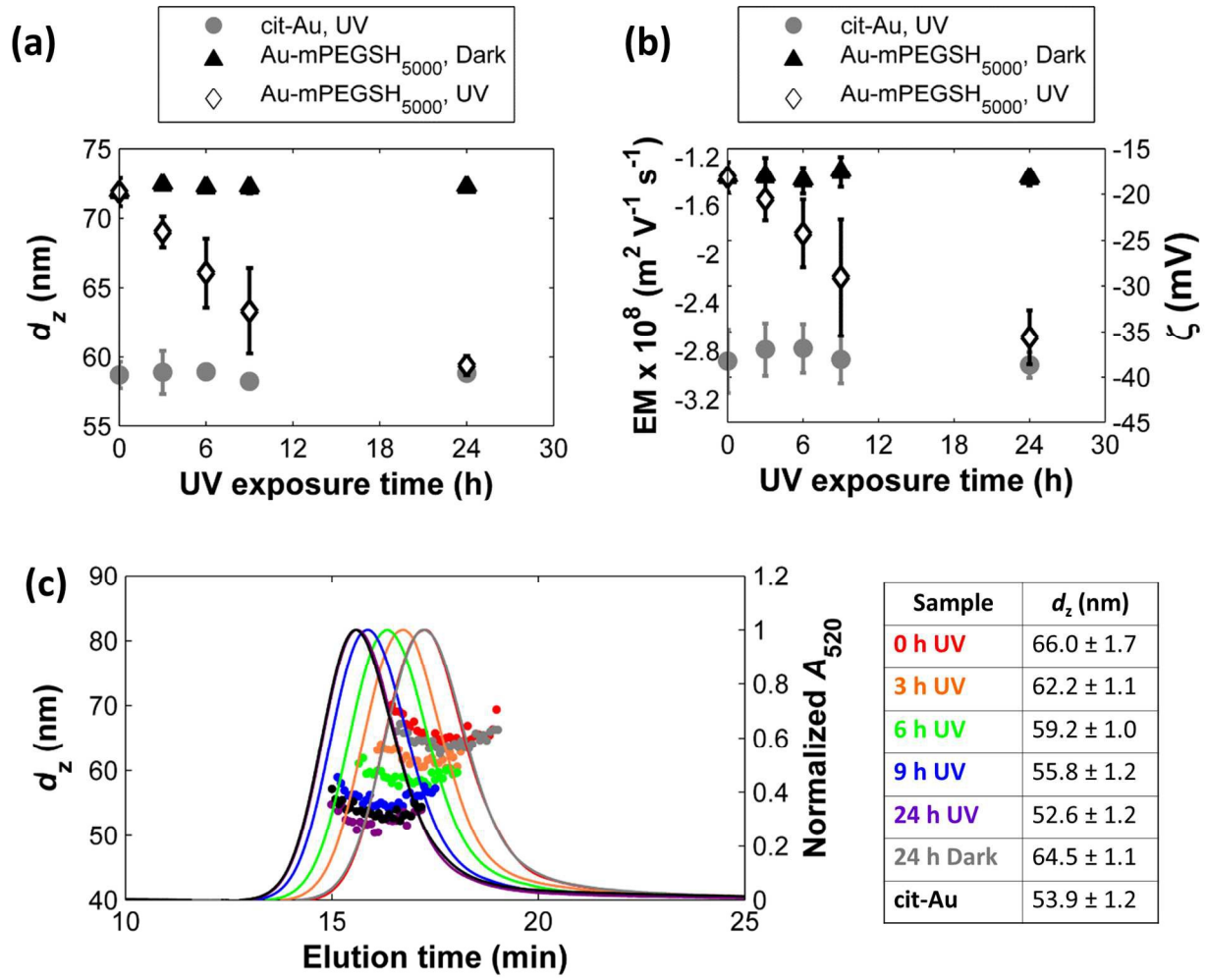

Figure 2. (a) d_z measured by batch DLS and (b) the EM or apparent ζ of the Au-mPEGSH$_{5000}$ NPs both decrease with UV exposure time, whereas no significant changes are observed for the dark Au-mPEGSH$_{5000}$ control or UV-exposed cit-AuNP control. The NPs were suspended in DI H_2O for the UV exposure, and DLS and EM were measured in 0.9 mM $NaHCO_3$ (pH 8). Values plotted are the average ± one standard deviation of measurements for at least three independently prepared samples. (c) d_z was also measured by A4F coupled with online UV-vis absorbance and DLS detectors, and a similar trend of decreasing d_z with UV exposure time was observed. A_{520} (normalized to the maximum absorbance) and d_z are represented by lines and dots, respectively. The d_z measurements shown in the figure correspond to data taken across the full width at half maximum of the light scattering peak (not shown). The table reports the average ± one standard deviation of the d_z measurements displayed on the plot. Au-mPEGSH$_{5000}$ NPs were prepared using the more highly reduced mPEGSH stock (with DTT impurity).

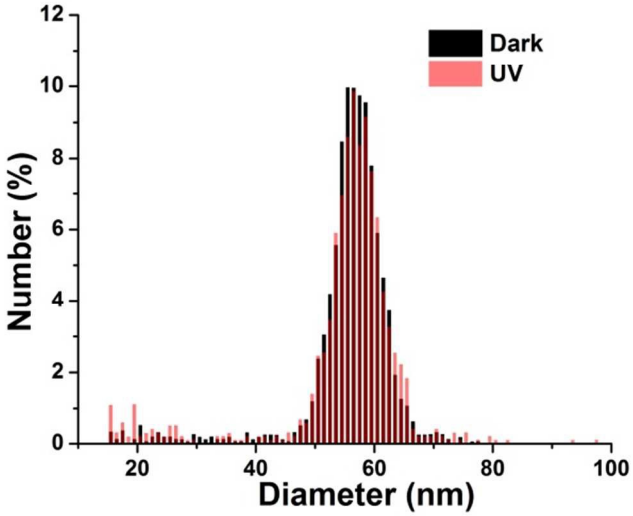

Figure 3. Core size distribution measured by spICP-MS shows no significant change for Au-mPEGSH$_{5000}$ NPs after 24 h UV exposure compared with the 24 h dark control. Data represent the average of two measurements per sample. Au-mPEGSH$_{5000}$ NPs were prepared using the more highly reduced mPEGSH stock (with DTT impurity).

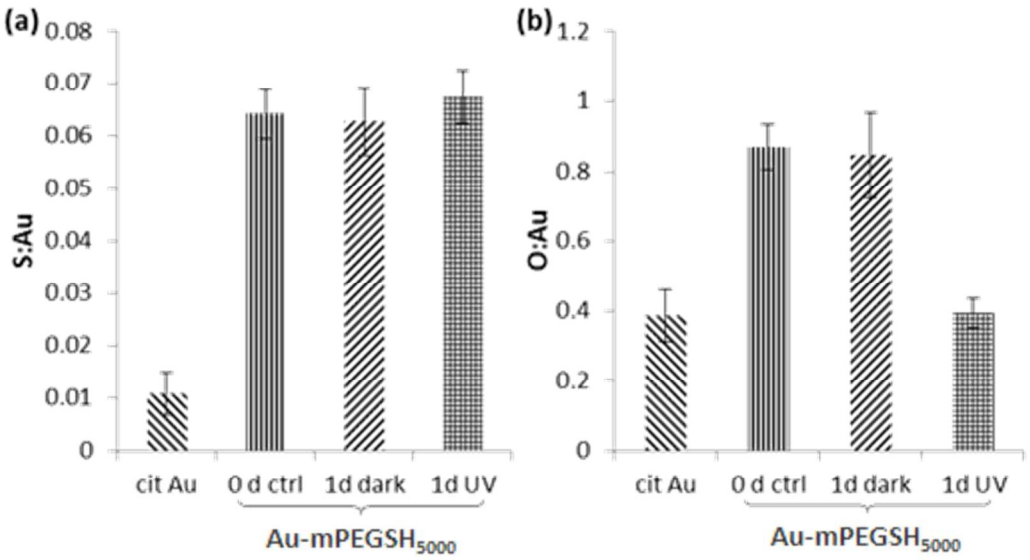

Figure 4. XPS analysis for the cit-Au NPs and Au-mPEGSH$_{5000}$ NPs (0 d control, 1 d dark, or 1 d UV) show (a) no significant change in S content for the Au-mPEGSH$_{5000}$ NPs after 24 h UV irradiation or dark storage, whereas (b) O content decreases upon 24 h UV exposure but not in the dark control. Values plotted are the average ± one standard deviation of at least three measurements. Au-mPEGSH$_{5000}$ NPs were prepared using the partially oxidized mPEGSH stock (without DTT impurity).

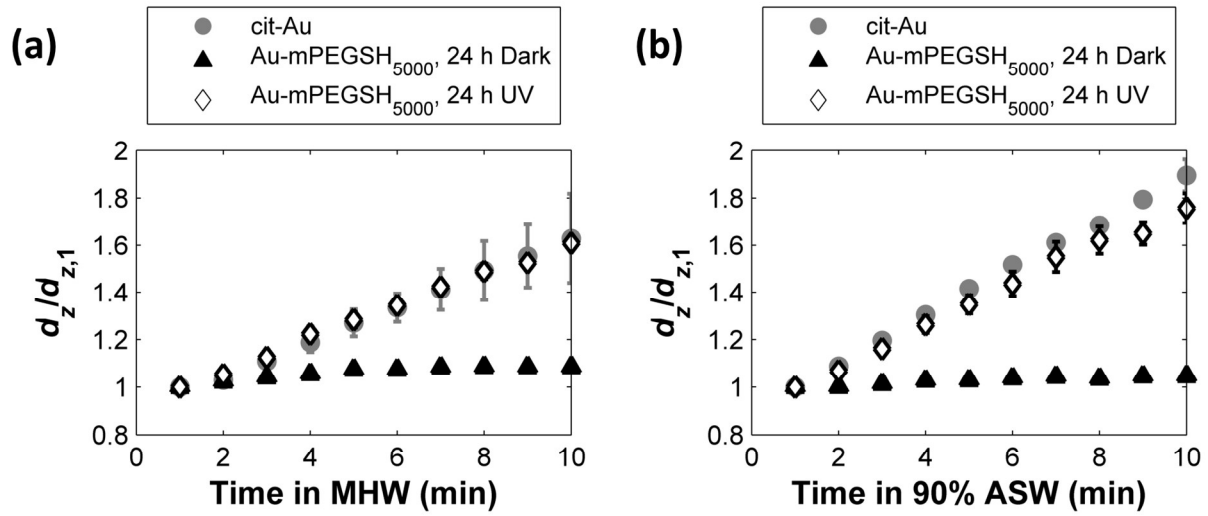

Figure 5. Time-resolved DLS measurements of the aggregation of the transformed Au-mPEGSH$_{5000}$ and control AuNPs in (a) moderately hard water and (b) 90 % artificial seawater. Each measured d_z is normalized to the first measurement ($d_{z,1}$). Au-mPEGSH$_{5000}$ NPs kept in the dark show relatively good stability in both media, whereas the UV-exposed Au-mPEGSH$_{5000}$ NPs show similar aggregation behavior to that of the cit-AuNPs. Values plotted are the average ± one standard deviation of measurements from three independently prepared samples. Au-mPEGSH$_{5000}$ NPs were prepared using the more highly reduced mPEGSH stock (with DTT impurity).

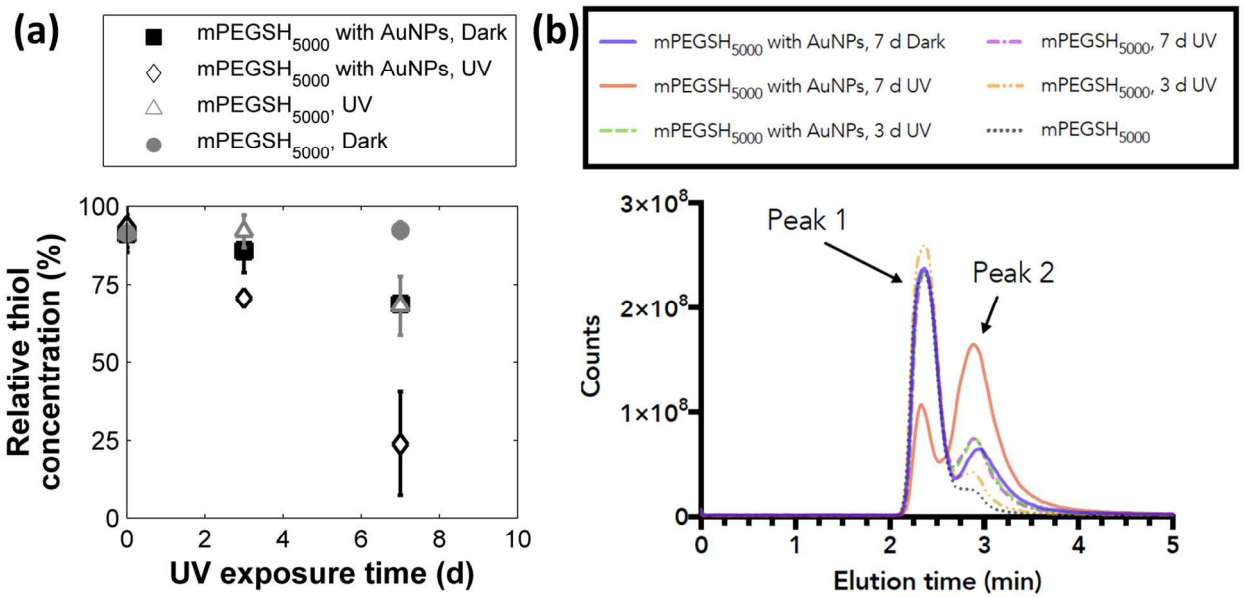

Figure 6. (a) Decreases in the thiol concentration (measured by Ellman's assay) in $mPEGSH_{5000}$ solutions suggest thiol oxidation in the presence of UV irradiation and the Au-$mPEGSH_{5000}$ NPs. (b) LC-MS shows two peaks in the chromatogram for total ion count, with the highest relative contribution of Peak 2 in the presence of the UV-irradiated Au-$mPEGSH_{5000}$ NPs. In the legends, "$mPEGSH_{5000}$ with AuNPs" denotes the supernatant containing ≈ 100 mg L^{-1} of $mPEGSH_{5000}$ after pelleting the AuNPs by centrifugation. In (a), relative thiol concentrations are calculated from the measured absolute molar concentrations as a percentage of the nominal initial molar concentrations (20 μmol L^{-1}). Values plotted in (a) are the average ± one standard deviation of measurements from three independently prepared samples. Samples were prepared using the more highly reduced mPEGSH stock (with DTT impurity), and samples for LC-MS were reacted with DTNB immediately after collection.

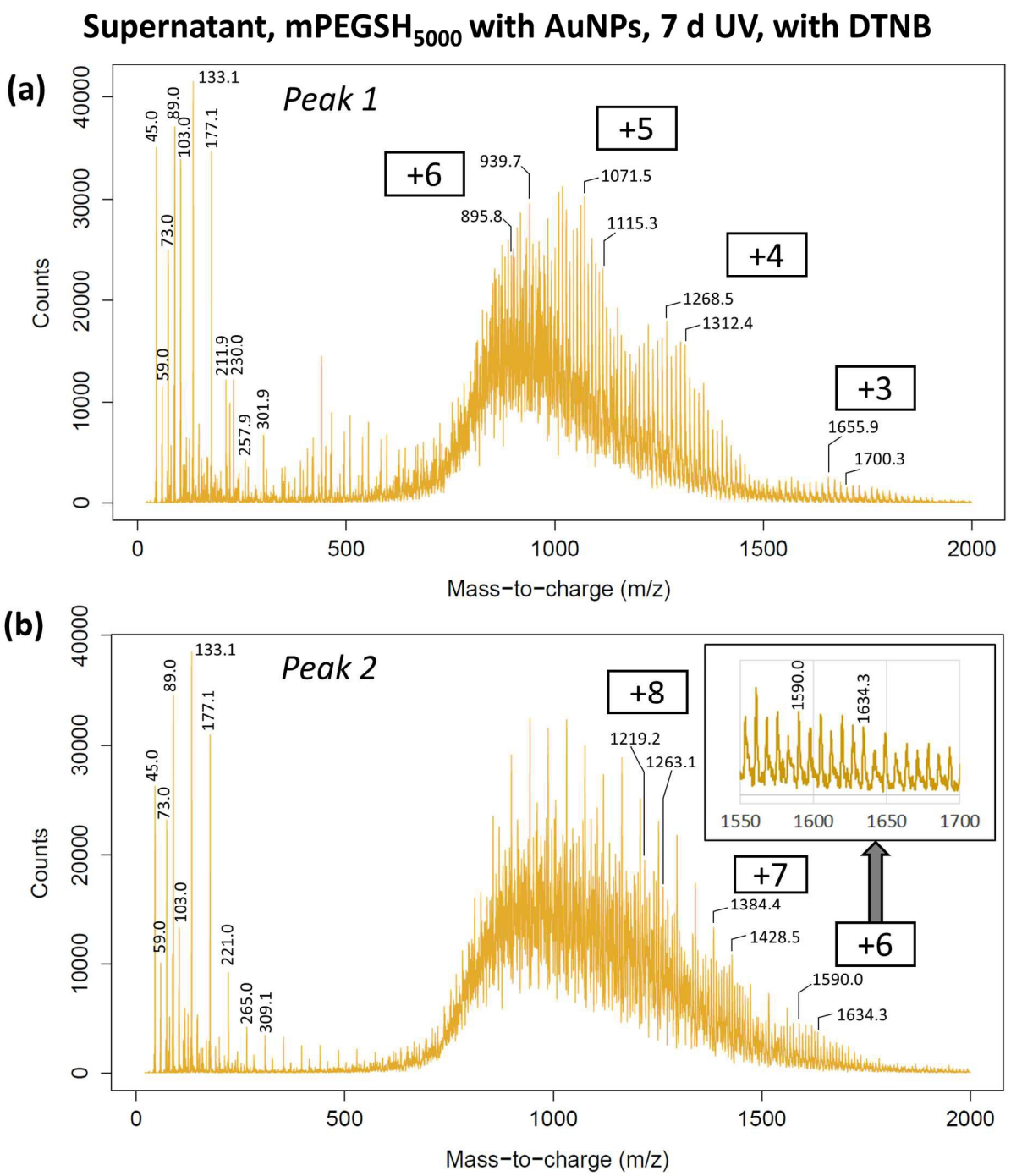

Figure 7. Mass spectra for (a) thiols and (b) disulfides in the supernatant of the pelleted Au-mPEGSH$_{5000}$ (in 100 mg L^{-1} mPEGSH$_{5000}$) after 7 d of UV irradiation and reaction with DTNB. Peaks 1 and 2 are labeled on Figure 6. Charge states (labeled in boxes) were determined from the peak spacing; the inset in (b) expands the spectrum for the +6 charge state. No significant shift in the *m*/*z* distribution of the main peaks (with charge states labeled) was observed compared to the mPEGSH control solution (SI Figure S8). Species with *m*/*z* < 600 are attributed to carbocations produced by in-source fragmentation of the polymer (SI Table S4) and other fragments or impurities that do not appear in complementary samples without DTNB tagging (SI Figure S9). Samples were prepared using the more highly reduced mPEGSH stock (with DTT impurity).